dELTA-MS: a mass spectrometry-based proteomics approach for identifying ADP-ribosylation sites and forms

Uribe, I.R.; Zahn, E.; Searfoss, R.; Kim, H.B.; Dasovich, M.; Voorneveld, J.; ... ; Leung, A.K.L.

Journal of proteome research

pubs.acs.org/jpr

Article

dELTA-MS: A Mass Spectrometry-Based Proteomics Approach for Identifying ADP-Ribosylation Sites and Forms

Isabel R. Uribe, Emily Zahn, Richard Searfoss, Han-Byeol Kim, Morgan Dasovich, Jim Voorneveld, Sabrina R. Hunt, Ugochi C. Onuoha, Catherine Valadez, Dmitri V. Filippov, Chan Hyun Na, Benjamin A. Garcia, Benjamin C. Orsburn,* and Anthony K. L. Leung*

Cite This: *J. Proteome Res.* 2025, 24, 1791−1803

Read Online

ACCESS | Metrics & More | Article Recommendations | Supporting Information

ABSTRACT: ADP-ribosylation, characterized by the addition of adenosine diphosphate ribose, can occur in both monomeric (MARylation) and polymeric (PARylation) forms. Little is known about the specific contributions of MARylation and PARylation to cellular processes due to a lack of tools for jointly investigating these individual forms. We present a novel mass spectrometry (MS)-based proteomics approach that preserves information about the native ADP-ribosylation form associated with the modification site within a single proteomics experiment. Our workflow enables the simplified, binary identification of ADP-ribosylation forms, avoiding some challenges typically presented by PARylated peptides during MS analysis. Our method uses the coronaviral enzyme NS2 to reverse our previous labeling approach, ELTA, which enzymatically labels the terminal ADP-ribose. NS2 deconjugates ELTA-labeled free or peptide-conjugated ADP-ribose monomers and polymers (thereby termed dELTA), leaving behind a signature phosphate. Our dELTA-MS workflow involves ELTA labeling, dELTA deconjugation, and further processing using *Deinococcus radiodurans* poly(ADP-ribose) glycohydrolase (DrPARG), resulting in two distinct mass shifts for MARylation and PARylation sites. We demonstrate the feasibility of this workflow for proteomics analyses using proof-of-principle peptide standards. dELTA-MS thus creates possibilities to reveal the fundamental biology of ADP-ribosylation and explore its dysregulation, in terms of both sites and forms, associated with disease progression.

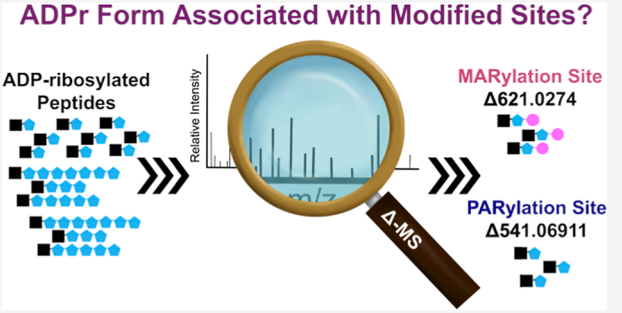

KEYWORDS: *proteomics, PARPs, ADP-ribosylation, mono-ADP-ribosylation, poly-ADP-ribosylation, post-translational modification*

INTRODUCTION

ADP-ribosylation—the addition of one or more ADP-ribose units—is a multifaceted post-translational modification that regulates essential cellular processes, including DNA repair, protein degradation, and stress responses.[1−4] ADP-ribosylation exists in two forms: mono-ADP-ribosylation (MARylation), where a single ADP-ribose is added per residue, or poly-ADP-ribosylation (PARylation), where multiple ADP-ribose units are added. MARylation can alter the conformation or charge of modified proteins, providing a new surface for protein−protein interactions.[1] In contrast, synthesis of poly(ADP-ribose) (PAR) results in a highly negatively charged polymer that can act as a scaffold to bind proteins and facilitate the formation of protein complexes or biomolecular condensates.[3,5]

ADP-ribosylation is synthesized by ADP-ribosyltransferases commonly known as PARPs,[6] and is degraded by glycohydrolase, such as PAR glycohydrolase (PARG).[1−4] The interplay between these enzymes makes ADP-ribosylation a dynamic and reversible protein modification. The site and form are two critical parameters of the "PAR code" that may direct biological outcomes in cells.[5,7] For example, a protein cofactor called Histone PARylation Factor 1 (HPF1) creates a new active site for PARP1,[8,9] which then switches its amino acid specificity from aspartate and glutamate to serine,[8,9] reduces the length of PAR it synthesizes[10,11] and promotes modification of histones instead of automodification of PARP1.[9,10] *In vitro* assays have shown that DNA repair proteins have different binding affinities for different lengths of PAR.[5,12−14] PARG also regulates the ADP-ribosylation form during DNA damage by processing down protein PARylation to MARylation.[15] Disruption of the balance between ADP-ribosylation's synthesis and degradation results in human diseases, from cancer to neurodegeneration.[1−4]

Received: October 4, 2024
Revised: December 18, 2024
Accepted: January 23, 2025
Published: March 13, 2025

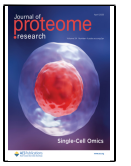

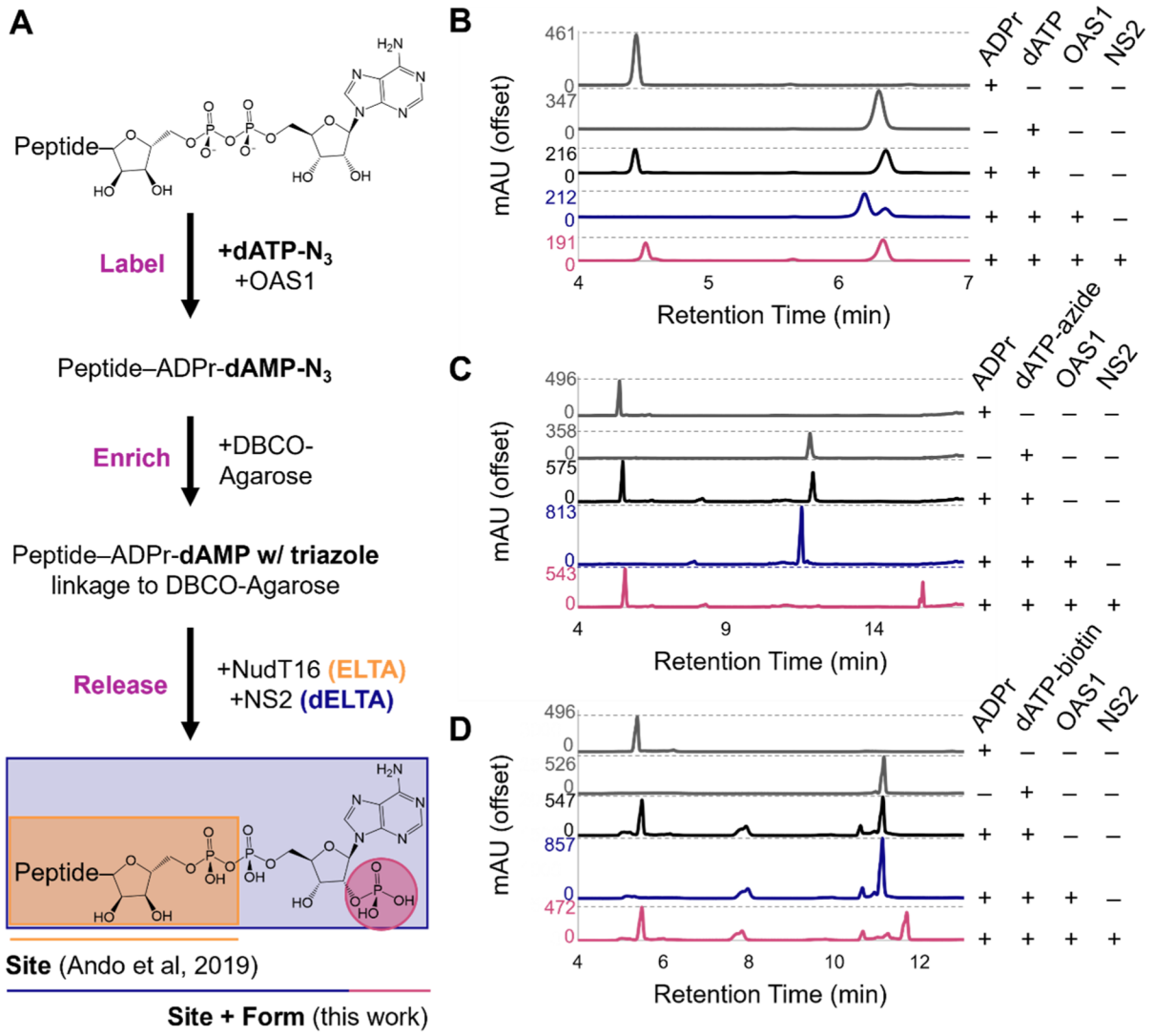

E

Reaction	Calculation	dATP	dATP-azide	dATP-biotin
OAS1 labeling	% Consumption of ADPr	100	98.7	92.8
NS2 reaction	% Consumption of ADPr-dAMP	100	98.9	79.3

Figure 1. NS2 deconjugates ELTA-labeled ADP-ribose. (A) Comparison of ELTA-MS with dELTA-MS. Both workflows use the same click chemistry-based enrichment system which enzymatically labels the terminal ADP-ribose with an azido-based enrichment tag that can be clicked to an alkyne-based resin. However, the workflows differ in the release step. ELTA-MS uses NudT16 which cleaves phosphodiester bonds within ADP-ribose, leaving behind a phospho-ribose mass tag. In contrast, dELTA-MS uses NS2 which cleaves the linkage between the terminal ADP-ribose and the azido enrichment tag, thus releasing peptides while preserving the integrity of the ADP-ribosylation. HPLC analysis of ADP-ribose ELTA-labeled by OAS1 with 1 mM dATP (B), 500 μM dATP-azide (C), and 125 μM dATP-biotin (D). These OAS1 products were then treated with NS2.

Several mass spectrometry (MS)-based proteomics methods[16−20]—including those from our lab[11,21]—have been developed to enrich and identify endogenous ADP-ribosylated substrates.[22,23] Interestingly, these methods have identified ADP-ribosylation on nine different amino acids, including aspartate and glutamate,[18] lysine and arginine,[21] cysteine,[20,24] and serine.[9] However, all of these methods do not determine whether the site was originally mono- or poly(ADP-ribosyl)-ated, as they process down ADP-ribosylation to a small, unique mass tag for site identification.

For example, our ADP-ribosylation proteomics workflow ELTA-MS first uses an enzyme called OAS1 to enzymatically label the terminal ADP-ribose (ELTA) with an azido-based enrichment tag.[11,25] These ELTA-labeled ADP-ribosylated peptides are then covalently pulled down with dibenzocyclooctyne-beads through click chemistry (Figure 1A). After stringent washing, we use an enzyme called NudT16 (Figure 1A, ELTA)—which cleaves the phosphodiester bonds within each ADP-ribose unit—to release peptides with a phospho-ribose tag[26] (Figure 1A, ELTA). Although MS analysis of these phospho-ribosylated peptides allows us to identify modification

https://doi.org/10.1021/acs.jproteome.4c00890
J. Proteome Res. 2025, 24, 1791−1803

sites, the digestion of ADP-ribose units by NudT16 removes information about the native form of ADP-ribosylation from the site identification.

To overcome this limitation, we propose modifying our ELTA-MS proteomics workflow, which enriches substrates in their native forms of ADP-ribosylation, to release ADP-ribosylated peptides while preserving the modification. Our workflow takes advantage of the substrate promiscuity of mammalian OAS1, an enzyme that synthesizes 2′,5′-oligoadenylate during viral infection, to label the terminal ADP-ribose.[27,28] Some coronaviruses possess a nonstructural protein (NS2) that enzymatically targets the phosphodiester bond within 2′,5′-oligoadenylate, counteracting the mammalian host's immune system.[28,29] We hypothesized that the enzymatic activity of the viral NS2 could be repurposed to target the 2′,5′-phosphodiester linkage between the terminal ADP-ribose and the ELTA enrichment tag, thereby releasing peptides while maintaining the native form of ADP-ribosylation. We term this deconjugation process of the ELTA label "dELTA". Here, we report the development of dELTA to characterize the site and form of ADP-ribosylation on peptides (Figure 1A, site + form).

METHODS

Protein Expression and Purification

Human OAS1. Full-length human 2′,5′-oligoadenylate synthetase 1 (OAS1, UniProtKB P00973) was expressed in and purified from *Escherichia coli* BL21 (DE3) cells. Briefly, cells were transfected with pSAT1-HisSUMO-OAS1. HisSUMO-OAS1[11] was expressed for 16−24 h at 16 °C. HisSUMO-OAS1 was initially purified with a HisTrap column (Cytiva Life Sciences) then desalted into 20 mM HEPES pH 7.5, 300 mM NaCl, and 10% glycerol. Next, HisSUMO-OAS1 was incubated with SENP protease in a 50:1 w/w ratio of protein/SENP at 4 °C for 16 h without shaking to remove the HisSUMO tag. The untagged OAS1 was purified by reverse IMAC using HisPur Ni-NTA Resin (Thermo Fisher). Finally, OAS1 was desalted into 20 mM HEPES pH 7.5, 100 mM NaCl, 0.5 mM TCEP, and 10% glycerol, flash frozen, and stored at −80 °C until use.

MHV NS2. Nonstructural protein 2a from Murine coronavirus (strain A59) (NS2, UniProtKB P19738) was expressed in and purified from DE3 cells. Briefly, cells were transfected with pSAT1-HisSUMO-NS2. HisSUMO-NS2 was expressed for 16 h at 16 °C. HisSUMO-NS2 was first purified with HisPur Ni-NTA Resin (Thermo Fisher) followed by gel filtration using a HiLoad 16/60 Superdex 200 column. HisSUMO-NS2 was flash frozen in 20 mM Tris pH 7.5, 150 mM NaCl, 1 mM DTT, and 10% glycerol before storing at −80 °C until use.

DrPARG. Poly(ADP-ribose) glycohydrolase from*Deinococcus radiodurans*(DrPARG) was expressed in and purified from DE3 cells. Briefly, cells were transfected with pET28a-DrPARG.[30] HisSUMO−DrPARG was expressed for 16−24 h at 16 °C. DrPARG was first purified with HisPur Ni-NTA Resin (Thermo Fisher) followed by gel filtration using a HiLoad 16/60 Superdex 200 column. DrPARG was flash frozen in 20 mM HEPES, 100 mM NaCl, 5 mM DTT, and 10% glycerol before storing at −80 °C until use.

Synthetic ADP-Ribosylated Peptide Preparation

Preparation of MARylated Peptides. JV-099 [Ac-PAKS(ADPr)APAPKKG-am] and JV-522 [Ac-GKS(ADPr)-GAALSKKG] (bold indicates heavy-labeled lysine) were synthesized and purified as previously described.[31,32]

Preparation of PARylated Peptide. Unmodified histone H3 peptide residues 1−20 (sequence: ARTKQTARKSTGG-KAPRKQL) with C-terminal acyl hydrazide was purchased from Motif Biotech. ADP-ribosylation of residue S10 was performed enzymatically using PARP1.[33] PARP1 was expressed and purified as previously described.[33]

Peptides were purified by RP-HPLC using a Waters Prep System and XBridge BEH C18 preparatory column with 0.1% trifluoroacetic acid in water (solvent A) and 95% acetonitrile, 0.1% trifluoroacetic acid in water (solvent B) as the mobile phases. The H3(1−20)S10arn mixture was purified using an elution gradient of 5−35% B over 34 min. Peptides were characterized by LC/MS using a Thermo Scientific LTQ XL with Easy nLC equipped with an Acclaim PepMap100 column.

HPLC Assay to Study NS2 Deconjugation of ADPr and dATP Analogs

1 mM ADPr was ELTA-labeled with equimolar dATP or dATP-azide and 250 μM ADPr was ELTA-labeled with equimolar dATP-biotin. All ELTA reactions were performed for 1 h at 37 °C with 2 μg low molecular weight poly(I/C) and 2 μg OAS1 in 1× OAS1 buffer (20 mM Tris pH 7.5, 20 mM magnesium acetate, and 2.5 mM DTT). Then 500 μM of ADPr-dAMP or ADPr-dAMP-azide or 125 μM of ADPr-dAMP-biotin was treated with 5 μg of NS2 in 1× NS2 Buffer (20 mM Tris pH 7.5, 50 mM NaCl, 5 mM NaCl, and 100 μM TCEP) for 2 h at 37 °C.

Samples were then analyzed on an Agilent 1260 Infinity II LC system with an InfinityLab Poroshell 120 EC-C18 column (particle size 2.7 μm, 4.6 × 100 mm) using two mobile phases. Mobile phase A consisted of 100 mM triethylammonium acetate pH 7.5 and mobile phase B consisted of 100% acetonitrile. Samples were passed through 0.45 μm nylon membrane syringe filters and then 2 nmol of each sample were injected. dATP-based samples were analyzed with an isocratic gradient of 5% B over 10 min. Samples with dATP-azide and dATP-biotin were analyzed with an isocratic gradient of 10% B over 5 min and then 30% B over 5 min. Peak areas were integrated using Agilent's OpenLab ChemStation software. OAS1 labeling yields were calculated based on "consumption" of the ADPr peak, using the peak areas for ADPr in the −OAS1 control and the +OAS1 reaction. NS2 deconjugation yields were calculated based on "consumption" of the ADPr-dAMP analog peak, using the peak areas for ADPr-dAMP in the +OAS1 reaction and the +NS2 reaction.

Analysis of NS2 Signature Phosphate

MALDI-TOF Analysis of MARylated Peptide. 200 μM JV-099 was labeled with 5-fold molar excess (1 mM) of dATP-azide using 1.4 μg OAS1 and 1.25 μg low molecular weight poly(I/C) in 1× OAS1 buffer at 37 °C for 1 h. Then, 100 μM JV-099-dAMP-azide (OAS1 product) was treated with 8.3 μg of NS2 in 1× NS2 buffer at 37 °C for 2 h.

Prior to MALDI-MS analysis, samples were cleaned up on homemade C18 Stage Tips using 2 C18 plugs and 200 μL micropipette tips. Stage Tips were conditioned with 50 μL 0.1% TFA in 80% acetonitrile in water (buffer B) and equilibrated with 50 μL 0.1% TFA (buffer A) before being loaded with the sample in a 1:5 (v/v) ratio of sample/buffer A. After washing the Stage Tips with 100 μL buffer A, samples were eluted with 10 mg/mL 2,5-dihydroxybenzoic acid (DHB) matrix in 0.1% TFA + 80% acetonitrile solution. About 500

https://doi.org/10.1021/acs.jproteome.4c00890
J. Proteome Res. 2025, 24, 1791−1803

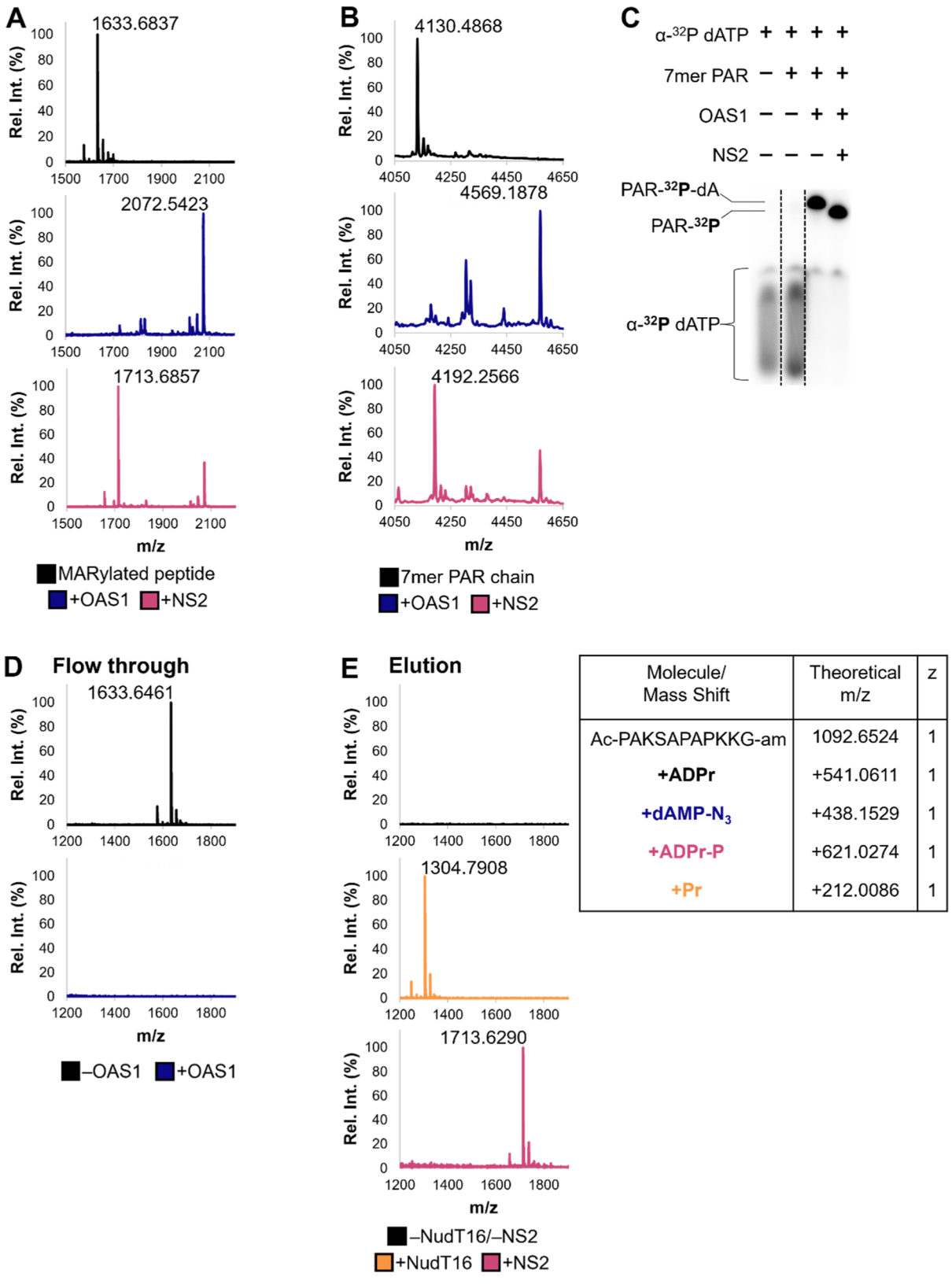

Molecule/ Mass Shift	Theoretical m/z	z
Ac-PAKSAPAPKKG-am	1092.6524	1
+ADPr	+541.0611	1
+dAMP-N_3	+438.1529	1
+ADPr-P	+621.0274	1
+Pr	+212.0086	1

Figure 2. NS2 leaves behind a signature phosphate on the terminal ADP-ribose. (A) MALDI-TOF mass spectra of ELTA-labeled JV-099 treated with NS2. (B) MALDI-TOF mass spectra of an ELTA-labeled 7mer PAR chain treated with NS2. (C) 15% urea-PAGE analysis of 7mer PAR ELTA-labeled with [α-^{32}P]-dATP and then treated with NS2. Dotted lines indicate two lanes that were removed for clarity. (D) MALDI-TOF mass spectra of the flowthrough for the controls of the click chemistry-based pulldown of JV-099. (E) MALDI-TOF mass spectra of the flowthrough after release of JV-099 via incubation of DBCO-agarose with NS2 and the positive control NudT16.

https://doi.org/10.1021/acs.jproteome.4c00890
J. Proteome Res. 2025, 24, 1791−1803

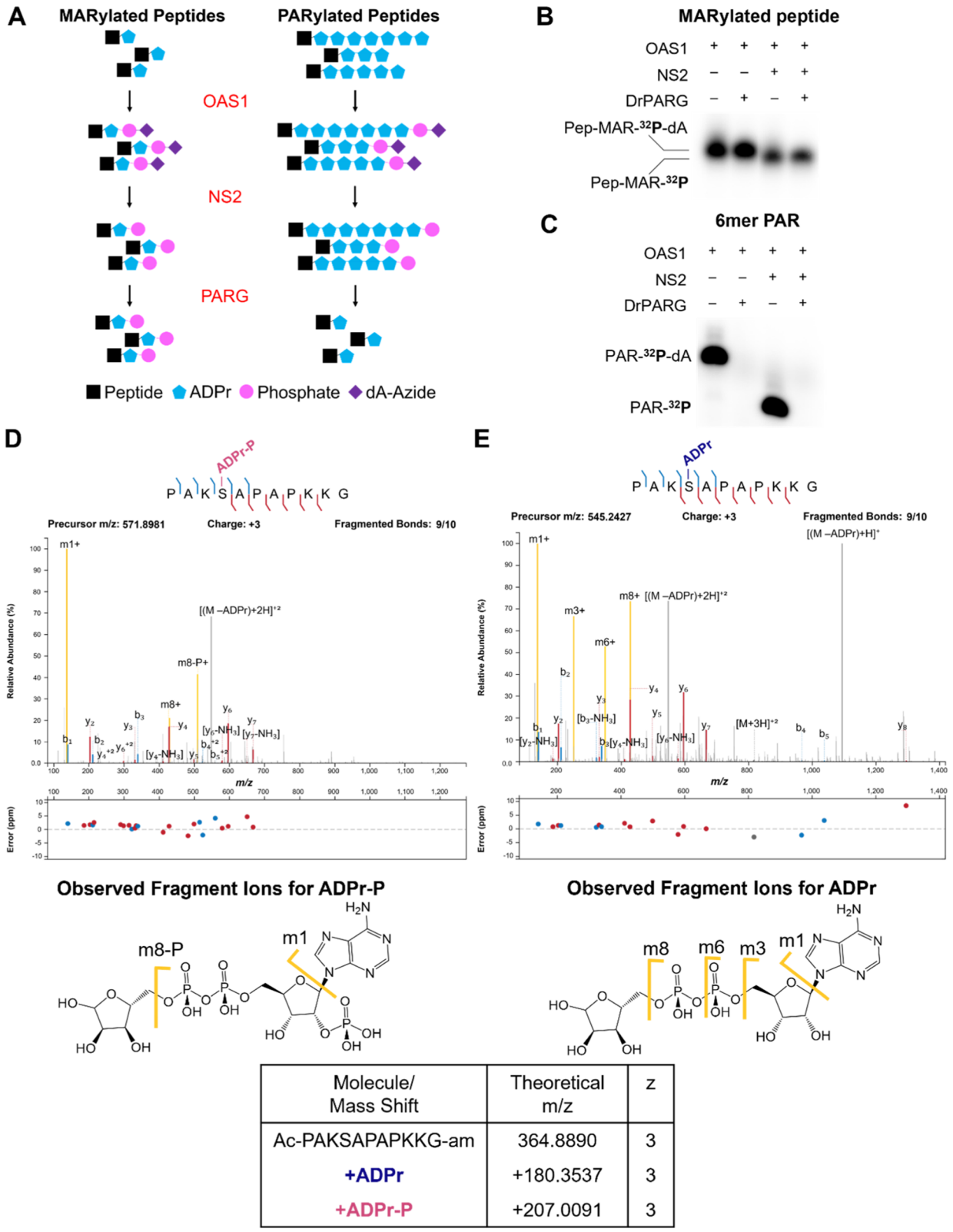

Molecule/ Mass Shift	Theoretical m/z	z
Ac-PAKSAPAPKKG-am	364.8890	3
+ADPr	+180.3537	3
+ADPr-P	+207.0091	3

Figure 3. PARG treatment after OAS1 and NS2 treatment preserves the phosphate on a MARylated peptide. (A) Workflow of enzymatic reactions. (B) Autoradiogram of enzymatic workflow on JV-099 labeled with [α-^{32}P]-dATP. (C) Autoradiogram of enzymatic workflow on a 6mer PAR chain labeled with [α-^{32}P]-dATP. (D) HCD MS2 spectrum of JV-099 with ADPr-P modification. (E) HCD MS2 spectrum of JV-099 with ADPr modification.

pmol of peptide was spotted for each reaction. Samples were analyzed by a Voyager DE-STR MALDI-TOF in the positive-ion, reflector mode (accelerated at 20 kV with 60%−75% grid and 130−150 ns extraction delay time).

https://doi.org/10.1021/acs.jproteome.4c00890
J. Proteome Res. 2025, 24, 1791−1803

MALDI-TOF Analysis of 7mer PAR Chain. 4 μM 7mer PAR chain was labeled with 10 μM dATP-azide using 2 μg OAS1 and 2 μg low molecular weight poly(I/C) in 1× OAS1 Buffer at 37 °C for 1 h. Then, 2.4 μM PAR-dAMP-azide (OAS1 product) was treated with 5 μg of NS2 in 1× NS2 Buffer at 37 °C for 2 h.

Prior to MALDI-MS analysis, samples were cleaned up on homemade C18 Stage Tips using 2 C18 plugs and 200 μL micropipette tips. Stage Tips were conditioned with 50 μL 50% ACN in water and equilibrated with 50 μL 100 mM TEAA pH 7 (buffer A) before being loaded with the sample in a 1:3 (v/v) ratio of sample/buffer A. After washing the Stage Tips with 100 μL buffer A and then 100 μL mQ H_2O, samples were eluted with 8:1 ratio of 10 mg/mL 2',4',6'-trihydroxyacetophenone (THAP) matrix in 50% acetonitrile and 50 mg/mL diammonium citrate in water. About 17 pmol of PAR was spotted for each reaction. Samples were analyzed by a Voyager DE-STR MALDI-TOF in the negative-ion, reflector mode (accelerated at 20 kV with a 80% grid and 600 ns extraction delay time).

Urea PAGE Analysis of NS2 Phosphate Signature. Substrates were ELTA-labeled with 1−4 μCi of [α-^{32}P]-dATP and then deconjugated with NS2 with the enzymatic reaction conditions listed above. Where indicated, samples were further processed with 10 μM DrPARG in 1× NS2 buffer at 37° for 1 h. Samples were diluted in 2× PAR loading buffer with dye (50% urea, 25 mM NaCl, 2 mM EDTA, 0.1% xylene cyanol, 0.1% bromophenol blue) and heated at 90 °C for 5 min. Samples were then loaded onto 10% urea gels and run at 800 V for 30 min (data in Figure 2) or 2 h (data in Figure 3) in 1× TBE running buffer (89 mM Tris, 89 mM Boric acid, 2 mM EDTA). Gels were imaged with a Typhoon FLA7000 machine (GE Healthcare).

LC−MS/MS Analysis of NS2 Phosphate Signature. 12 μM JV-099 was labeled with 24 μM dATP-azide using 2 μg OAS1 and 2 μg low molecular weight poly(I/C) in 1x OAS1 Buffer at 37 °C for 1 h. The OAS1 reaction was diluted 2-fold for the NS2 reaction, consisting of 6.75 μg NS2 in 1× NS2 buffer at 37 °C for 2 h. This NS2 reaction was then diluted 2-fold for the DrPARG reaction, consisting of 10 μM DrPARG in 1× NS2 buffer at 37 °C for 1 h. 10% trifluoroacetic acid (TFA) was added to samples to a final concentration of 1% TFA and then samples were loaded onto homemade Stage-Tips that were conditioned with 80% ACN/0.1% TFA and equilibrated with 5% ACN/0.1% TFA. Peptides were washed with 0.1% TFA, eluted with 40% ACN, and dried down to completion by vacuum centrifugation.

JV-099 was analyzed on a Thermo Orbitrap Fusion Lumos mass spectrometer coupled to an Ultimate3000 RSLCnano nanoflow liquid chromatography system (Thermo). The peptides were loaded onto a trap column (Acclaim PepMap 100, LC C18, 5 μm, 100 μm × 2 cm, nanoViper) at a flow rate of 8 μL/min and resolved on an analytical column (Easy-Spray PepMap RSLC C18, 2 μm, 75 μm × 50 cm) at a flow rate of 0.3 μL/min. LC buffer A was 0.1% formic acid (FA), LC buffer B was 0.1% FA/95% ACN, and the column oven was maintained at 40 °C. Peptides were separated with a 95 min gradient from 8% to 27% buffer B, followed by an increase to 50% buffer B over 5 min, another increase to 90% buffer B over 5 min, and finally a 10 min washing block. MS data was collected with a Thermo Orbitrap Fusion Lumos Tribrid mass spectrometer with a spray voltage of 2.4 kV, capillary temperature of 200 °C, and RF lens of 30%. MS1 scans were performed at a resolution of 120k, a scan range of 300 to 1800 m/z, a maximum injection time of 50 ms, and an automatic gain control (AGC) target of 1,000,000 charges. Precursor ions were isolated with a width of 1.6 m/z, an AGC target of 50,000 charges. HCD fragmentation was performed with a normalized collision energy of 25% and a resolution of 30k. Peptide spectral matches were identified as described below.

dELTA-MS Workflow

Small Scale Enrichment of MARylated Peptide Standard. 100 μM JV-099 was labeled with 250 μM dATP-azide using 5 μg OAS1 and 5 μg low molecular weight poly(I/C) in 1× OAS1 buffer at 37 °C for 1 h. Reaction volumes were brought up to 500 μL and then 100 μL of 50% DBCO-agarose equilibrated in 1× PBS was added to each OAS1 reaction before rotating end-over-end for 1 h at room temperature. The DBCO-agarose was pelleted and then the supernatant (flowthrough) was collected for MALDI-TOF analysis, followed by three 2-min washes of the agarose with 1× PBS. The DBCO-agarose was rinsed with 1× PDE buffer (100 mM HEPES pH 8.0, 15 mM $MgCl_2$) or 1× NS2 buffer and then no phosphodiesterase, 5 μg NudT16, or 25 μg NS2 was added in their respective buffers. The DBCO-agarose was incubated with these enzymes at 37 °C shaking at 1400 rpm for 2 h. The DBCO-agarose was pelleted and then the supernatant (elution) was collected for MALDI-TOF analysis. Samples were cleaned up on Stage-Tips and analyzed by MALDI-TOF as described above.

Cell Harvesting, Proteolysis, and Desalting for Proteomic Analyses. Cells were treated with 1 mM H_2O_2 for 10 min, washed with ice cold PBS once, and harvested and lysed in buffer containing 6 M guanidine hydrochloride, 100 mM HEPES pH 8.0, 5 mM tris(2-carboxyethyl)phosphine hydrochloride (TCEP-HCl), and 10 mM 2-chloroacetamide (CAM) preheated to 95 °C. Lysates were then mixed at 1000 rpm at 95 °C for 10 min in the dark. Total protein concentration of lysates was determined by Bradford assay. For the experiment with the MARylated peptide standard, 3 nmol of JV-522 was spiked into the lysate. Protein digestion reactions were prepared by diluting lysates containing 10 mg total protein 6-fold in 100 mM Tris−HCl pH 8.0 and adding 100 μg Trypsin (Thermo Fisher) and 100 μg LysC (Wako) and incubating overnight at 37 °C and shaking at 200 rpm. 1 M triethylammonium acetic acid (TEAA) pH 7 was added to peptide solutions to a final concentration of 100 mM before clarifying peptide solutions by centrifugation at 4000 rpm for 30 min at 4 °C. Peptides were desalted on 1 mg SepPak t-C18 Classic cartridges (Waters) conditioned with 80% acetonitrile (ACN) and equilibrated with 100 mM TEAA pH 7.5. Peptides were washed with 100 mM TEAA pH 7.5 and eluted with 40% ACN. Samples were dried down to completion by vacuum centrifugation.

Enrichment of ADP-Ribosylated Peptides with dELTA Workflow. ADP-ribosylated peptides were resuspended in miliQ H_2O and enriched using adapted versions of the labeling and enrichment steps of the ELTA-MS proteomics workflow.[11] For the experiment with the PARylated peptide standard, 6 nmol of H3(1−20)S10arn was spiked into each technical replicate. First, peptides were incubated with 100 μM N6-(6-Azido)hexyl-dATP (Jena Bioscience), 20 μg/mL low molecular weight poly(I/C), and 80 μg/mL OAS1 in buffer containing 100 mM Tris−HCl pH 7.5, 20 mM magnesium

https://doi.org/10.1021/acs.jproteome.4c00890
J. Proteome Res. 2025, 24, 1791−1803

acetate, and 2.5 mM dithiothreitol (DTT) for 1 h at 37 °C and shaking at 800 rpm. 100 μL of 50% DBCO-agarose equilibrated in 1× PBS was added to each OAS1 reaction before rotating end-over-end overnight at 4 °C. The samples were centrifuged to pellet the agarose resin and the supernatant (flow through) was discarded. The agarose resin was washed three times with 5 M NaCl, three times with 20% ACN, and three times with 1× PBS. After washing the resin twice in 1× NS2 buffer, the samples were transferred to new Eppendorf tubes. 80 μg of NS2 was added to each sample and then the volume was brought up to 200 μL using 1× NS2 buffer. Samples were incubated at 37 °C for 2 h shaking at 1400 rpm. The samples were centrifuged to pellet the agarose resin and 150 μL of the supernatant (elution) were transferred to new Eppendorf tubes. DrPARG was added to a final concentration of 10 μM to each sample followed by incubation at 37 °C shaking at 800 rpm for 1 h. Samples were stored at −80 °C until ready to remove excess enzymes via 10 kDa molecular weight cutoff filters.[9] 10% trifluoroacetic acid (TFA) was added to samples to a final concentration of 1% TFA and then samples were loaded onto homemade Stage-Tips that were conditioned with 80% ACN/0.1% TFA and equilibrated with 5% ACN/0.1% TFA. Peptides were washed with 0.1% TFA, eluted with 40% ACN, and dried down to completion by vacuum centrifugation.

LC−MS/MS Analysis of Enriched Standard Peptides. Peptides were separated on an Easy-Spray PepMap Neo C18 column, 75 μm by 150 mm at 300 nL/min and heated to 40 °C. A gradient of buffers A and B, consisting of 0.1% Formic acid in water and 0.1% Formic acid in acetonitrile, respectively, was applied from 6%−8% B for 0−5 min, 8%−27% B from 5 to 100 min, 27%−50% B from 100 to 105 min, 50%−90% B from 105 to 110 min, held at 90% B from 110 to 115 min, and equilibrated from 90%−5% B from 115 to 120 min. MS1 scans were conducted with a 3 s cycle time from 300 to 1750 m/z and Orbitrap resolution of 60 K, maximum inject time of 60 ms, and AGC target of 6×10^5. Candidates for MS2 analysis were selected from 350 to 1550 m/z with a minimum intensity of 2×10^4, charge states 3−5 and dynamic exclusion set to excluding targets for 30 s after 1 time of analysis. MS2 scans were performed using EThcD with a 50 ms reaction time, 1×10^6 reagent target, 200 ms maximum ETD reagent injection time, and supplemental activation set to true with 20% collision energy. The maximum precursor injection time was 120 ms with 2×10^5 AGC target and 400% normalized AGC target. Scans were performed with a 110 m/z fixed first mass, and 1 microscan was performed per target.

Peptide Spectral Matching for Standard Peptides. The theoretical precursor m/z for each standard peptide was calculated using the MS Fragment Ion Generator from the phpMS Demo Suite.[34] Mass shifts for ADPr-P (+621.0274), ADPr (+541.0611), N-terminal acetylation (+42.0106), C-terminal amidation (−0.9840), heavy lysine (+6.0201), and C-terminal acyl hydrazine (+14.0269) were indicated as necessary for each peptide sequence. Raw files were searched manually in XCalibur (Thermo Fisher) for the precursor m/z for potential peptide spectral matches (PSMs). Once identified, the peak list for the entire MS2 spectrum of the potential PSM was exported and then plotted in the Interactive Peptide Spectral Annotator (IPSA).[35] IPSA annotations were exported as svg files. Text placement was edited for readability and diagnostic ions for ADPr-P or ADPr were manually highlighted in the svg files.

Data Availability. Vendor LCMS raw files, MALDI spectra, and relevant meta-data have been deposited at the https://massive.ucsd.edu/ProteoSAFe/static/massive.jsp public repository as accession MSV000095991.

RESULTS

NS2 Deconjugates ELTA Labels from Mono(ADP-Ribose)

To assess the feasibility of incorporating NS2 into our enrichment workflow, we first studied the substrate specificity of NS2 on a protein-free monomeric ADP-ribose that was ELTA-labeled with various dATP analogs. OAS1 converts ADPr with dATP into a singular product of ADPr-dAMP via a 2′,5′-phosphodiester linkage.[11] As expected, all ADPr was converted by OAS1 to a new peak with a longer retention time (Figure 1B, blue; Figure 1E) and a small shoulder on the peak, corresponding to a slight excess of dATP. When the reaction was treated with NS2, which targets 2′,5′-phosphodiester linkages, two peaks were observed with retention times similar to the original standards of ADPr and dATP (Figure 1B, pink).

We also tested analogs of dATP under the same enzymatic reaction conditions. ADPr was ELTA-labeled with dATP-azide (Figure 1C, blue), which resulted in only a slight decrease in labeling efficiency compared to the reaction with dATP (Figure 1E). NS2 efficiently deconjugated the dAMP-azide group from ADPr (Figure 1C, pink; Figure 1E). For the bulkier dATP-biotin, although the efficiencies were lower, OAS1 was still able to label ADP-ribose with this analog and the modification was removed by NS2 (Figure 1D,E). Taken together, this HPLC assay demonstrated that NS2 can deconjugate ADP-ribose monomers from various dAMP analogs labeled by ELTA.

Interestingly, the peak corresponding to the expected dAMP analog product of NS2 cleavage (Figure 1C,D, pink) had a longer retention time relative to their respective dATP analog standards (Figure 1C,D, gray). In ion-paired reverse-phase liquid chromatography, the retention coefficient depends on the net charge and polarity of analytes.[36] Both dATP analogs have nonpolar alkyl linkers to azide or biotin groups, likely causing their higher retention compared to dATP. This is confirmed by the solvent gradient: dATP analogs require 30% acetonitrile for elution, while dATP elutes with just 10%. The observed difference in retention times suggests that the NS2 products may not be simply ADPr and the corresponding dAMP analog.

NS2 Deconjugates ELTA-Labeled ADP-Ribose, Resulting in a Signature Phosphate

Phosphodiester cleavage, such as breaking the RNA backbone, leaves the phosphate group on only one nucleoside, either at the 3′ or 5′ end.[37] Similarly, for 2′,5′-oligoadenylate, the natural substrate of NS2, the phosphate can remain on either the 2′ or 5′ end.[28,38] When NS2 uses ADPr-dAMP as a substrate, there are two possible outcomes: (1) the phosphate stays on the 5′ end, forming ADPr and dAMP[28] or (2) the phosphate stays on the 2′ end, forming ADPr-phosphate (ADPr-P) and deoxyadenosine (dA).[38] Based on the longer retention time for the second peak in the chromatograms of the NS2 reactions on the nonpolar C18 column compared to the dATP standards (Figure 1B−D), we hypothesized that the products were ADPr-P and the corresponding dA analogs, which is consistent with the lower polarity of dA (no phosphates) compared to dATP (three phosphates). Determining the phosphate location after NS2 cleavage is thus

https://doi.org/10.1021/acs.jproteome.4c00890
J. Proteome Res. 2025, 24, 1791−1803

critical for understanding the underlying mechanism and, more importantly, identifying the mass shift signature associated with the deconjugation process in our proteomic pipeline.

To unambiguously locate where the phosphate remained after NS2 cleavage, we turned to mass spectrometry-based analysis to characterize the NS2 deconjugation products. We performed MALDI-TOF analyses to track the location of the phosphate during the enzymatic reactions of a synthetic MARylated peptide (JV-099) (Figure 2A) and a protein-free 7mer PAR chain (Figure 2B) that were both ELTA-labeled with dATP-azide. Since MALDI is an ionization source that generates predominantly singly charged species, reacting JV-099 (Figure 2A, black) with OAS1 and dATP-azide resulted in the expected mass shift of 438, corresponding to the transfer of dAMP-azide to the ADP-ribose on the peptide (Figure 2A, blue). After NS2 deconjugation of the ELTA-labeled peptide, we expected a mass shift relative to the unlabeled MARylated peptide of 80 if the phosphate (PO_3) group remained with ADPr, as hypothesized. Indeed, we observed the mass shift of 80 (Figure 2A, pink), indicating that the phosphate remained on the 2′ end of ADPr after NS2 cleavage of the ADPr-dAMP linkage.

Similarly, OAS1 labeling of the PAR chain (Figure 2B, black) resulted in the expected mass shift of 438, corresponding to the dAMP-azide group transferred to the terminal ADP-ribose (Figure 2B, blue). However, after NS2 deconjugation of the ELTA-labeled PAR chain, we observed a mass shift of only 62 (Figure 2B, pink), instead of 80. Such a difference corresponds to the mass of H_2O, suggesting that the product may be a 2′,3′-cyclic phosphate. This interpretation agrees with a previous study showing that various 2′,5′-phosphodiesterases, including MHV NS2 used in this study, cleave the 2′,5′-oligoadenylates to produce a 2′,3′-cyclic phosphate terminus.[39] The different mass shift observed for the PAR chain and the MARylated peptide could be due to the difference in pH of the matrices used for each MALDI-TOF analysis. The very acidic condition (pH 2) of the 2,5-dihydroxybenzoic acid (DHB) matrix for peptides analyzed in the positive ionization mode may open up the cyclic phosphate through an acid-catalyzed hydrolysis mechanism, whereas the less acidic condition (pH 4) of the 2',4',6'-trihydroxyacetophenone (THAP) matrix may preserve the cyclic phosphate as the dominant product.

To confirm the presence of the signature phosphate left behind by NS2, we used an orthogonal urea PAGE assay with radioactive reagents. Since OAS1 transfers dAMP, including the α-phosphate, from dATP to the terminal ADPr, we tracked the α-phosphate using ^{32}P radioactivity. This labeling enabled us to observe whether NS2 cleavage of ADPr-dAMP results in the phosphate being left on the terminal ADPr or released as a dAMP group. OAS1 labeling of PAR with [α-^{32}P]-dATP produced PAR-dAMP, evident in the slower migration of the ^{32}P radioactive signal (Figure 2C; see also Figure S1). Notably, NS2 deconjugation of PAR-dAMP retained the signal from the radioactive α-phosphate and resulted in a slightly faster migration, presumably due to loss of the dA group. Thus, these two assays indicate that NS2 cleavage leaves behind a phosphate on the terminal ADPr of MAR and PAR.

To assess the feasibility of incorporating NS2 into our enrichment workflow, we tracked the synthetic MARylated peptide JV-099 through the labeling, pull down, and deconjugation steps via MALDI-TOF analysis. We first incubated JV-099 with dATP-azide in the presence and absence of OAS1. These reactions were then incubated with DBCO-agarose, and we sampled the supernatant. As expected, we did not detect JV-099 in the supernatant when OAS1 was present (Figure 2D, blue) as the dAMP-azide labeled peptides were likely captured by the DBCO resin. However, the peptide was identified in the supernatant when OAS1 was absent (Figure 2D, black). The DBCO-agarose was then incubated with NS2, NudT16 (a positive control for ELTA-MS), or no phosphodiesterase as a negative control, and the resultant supernatants were sampled again. As expected, we did not observe any peptide released into the supernatant when phosphodiesterase was not added (Figure 2E, black). We observed the expected m/z for the synthetic peptide sequence with a phospho-ribose tag following release by NudT16 (Figure 2E, orange). When NS2 was added to the DBCO-agarose, we observed an m/z corresponding to JV-099 with the signature phosphate (Figure 2E, pink). Although MALDI ionization is not conducive to robust quantification,[40] this qualitative assay confirmed that NS2 can be used to deconjugate an ELTA-labeled peptide with its ADP-ribosylation intact.

Generating Two Distinct Mass Tags to Distinguish between MAR and PAR Sites

For any particular peptide sequence, the varying length of ADP-ribosylation at the same site can reduce sensitivity during mass spectrometry analysis, as the signal is now spread across various m/z due in part to the heterogeneous lengths of negatively charged ADP-ribosylation. Therefore, all existing proteomics workflows process the ADP-ribosylation down to a unique mass tag for MS analyses. A commonly used method processes down PARylation using PARG to produce an ensemble of MARylated peptides.[41] To simplify MS analysis and utilize the signature phosphate left behind by NS2 deconjugation, we hypothesized that our workflow could incorporate treatment with *D. radiodurans* PARG (DrPARG), which is known to remove all but the ADP-ribose proximal to the peptide,[30] as the last step after OAS1 labeling and NS2 deconjugation. In this scenario, modification sites originally MARylated will possess the terminal phosphate after NS2 treatment, which we hypothesized to be insensitive to DrPARG treatment. Conversely, a labeled PARylated peptide with a terminal phosphate following NS2 deconjugation will be cleaved to a MARylated peptide after DrPARG treatment (Figure 3A).

To test the feasibility of this approach, we analyzed the consecutive OAS1, NS2, and PARG enzymatic reactions on monomeric and polymeric substrates. A synthetic MARylated peptide was first labeled by OAS1 with [α-^{32}P]-dATP (Figure 3B; see also Figure S2). Adding DrPARG to the OAS1 reaction did not reduce the phosphate signal, which is consistent with the published report that DrPARG does not cleave the ADP-ribose proximal to the peptide. Importantly, when DrPARG was added to the MARylated peptide after OAS1 and NS2 treatments—now marked with the additional radioactive phosphate—no decrease in radioactive signal was observed. Thus, DrPARG treatment of an NS2-deconjugated, ELTA-labeled MARylated peptide did not remove the signature phosphate.

As a control, we wanted to confirm that DrPARG could process down a polymer of ADP-ribose that possessed the signature phosphate. We next labeled a 6-mer PAR chain with [α-^{32}P]-dATP using OAS1 (Figure 3C; see also Figure S2).

https://doi.org/10.1021/acs.jproteome.4c00890
J. Proteome Res. 2025, 24, 1791−1803

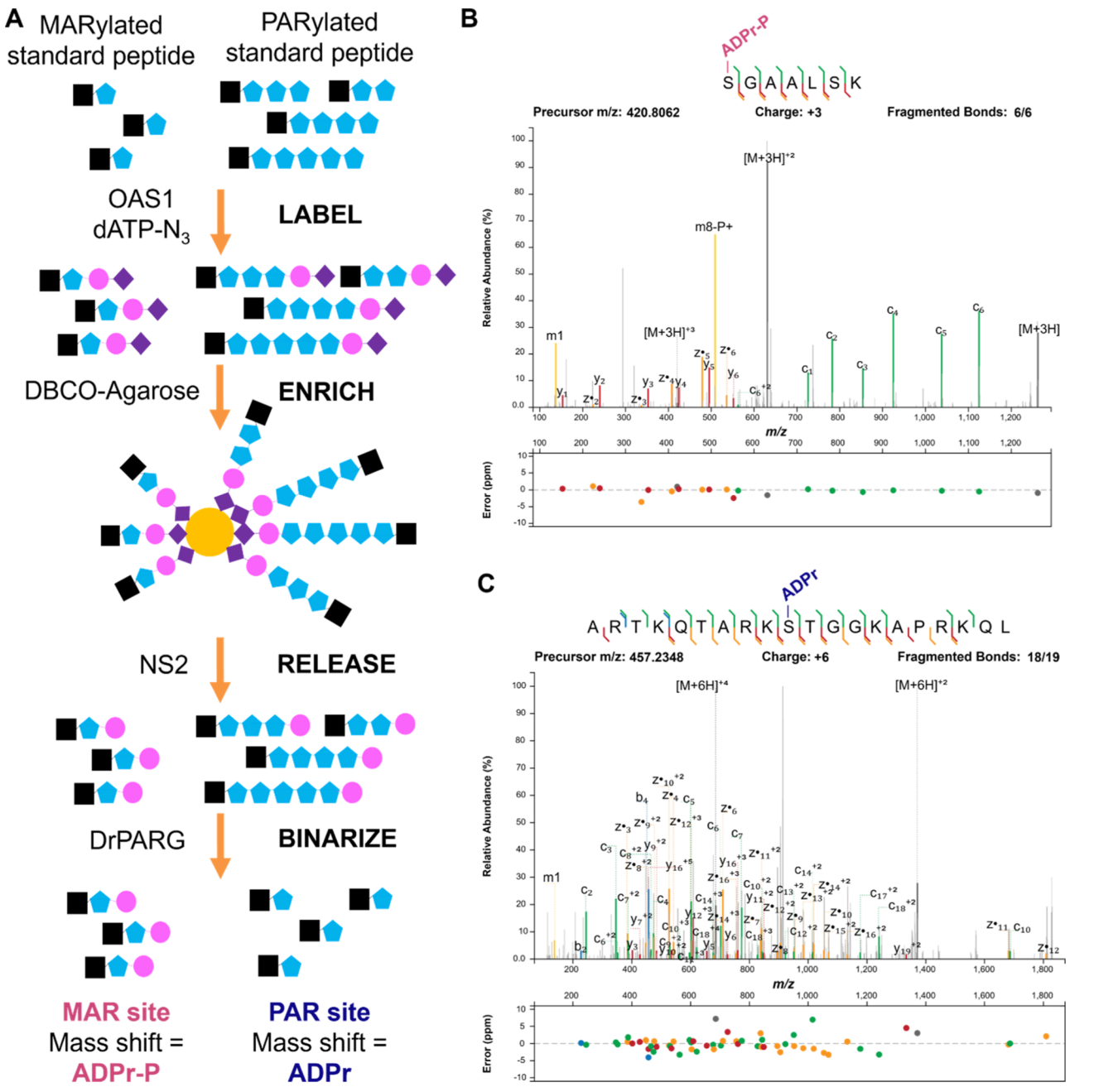

Figure 4. dELTA-MS workflow pulls down standard MARylated and PARylated peptides with unique mass tags. (A) Schematic of dELTA-MS workflow for proof-of-principle experiments to identify JV-522 and H3(1−20)S10arn. In one experiment, JV-522 was spiked into H_2O_2-treated HeLa cell lysate prior to digestion. In another experiment, H3(1−20)S10arn was spiked into H_2O_2-treated HeLa cell lysate peptides right before dELTA-MS. (B) EThcD MS2 spectrum of JV-522 that was identified with the ADPr-P modification expected for a MAR site after processing with the dELTA-MS workflow. (C) EThcD MS2 spectrum of H3(1−20)S10arn that was identified with the ADPr modification expected for a PAR site after processing with the dELTA-MS workflow.

This radioactive signal was lost after DrPARG treatment, confirming its ability to cleave the PAR chain into ADP-ribose monomers. As expected, NS2 deconjugation of the ELTA-labeled PAR resulted in further migration in the urea PAGE gel while retaining the terminal radioactive phosphate group (Figure 3C; cf. Figure 2C). DrPARG treatment of this processed PAR chain resulted in a complete loss of radioactivity, similar to the ELTA-labeled PAR. These data indicate that the presence of the terminal phosphate did not affect DrPARG's ability to process PARylated substrates to MARylation.

After obtaining biochemical confirmation that the consecutive OAS1, NS2, and PARG reactions produced two distinct signals on MAR and PAR (Figure 3A), we then tested whether we could detect a synthetic standard peptide modified with ADPr-P via liquid chromatography coupled to tandem mass spectrometry (LC−MS/MS). To generate the peptide with ADPr-P, we repeated the same triple-enzyme workflow on the MARylated peptide JV-099 (Figure 3A). We also processed the synthetic MARylated peptide through the same workflow, excluding the enzymes, to control for any possible hydrolysis of the ADP-ribose-based modifications.

https://doi.org/10.1021/acs.jproteome.4c00890
J. Proteome Res. 2025, 24, 1791−1803

In the representative MS2 spectrum for the MARylation site, we observed the m/z for the synthetic peptide sequence with the expected mass shift corresponding to ADPr-P (Figure 3D). In the representative MS2 spectrum for the control, we observed the m/z for the peptide with the mass shift of ADPr (Figure 3E). Sufficient fragments were obtained to allow sequence identity confirmations by HCD fragments as well as modification localization for both ADPr-P and ADPr motifs. Multiple diagnostic ions characteristic of ADP-ribose were observed in the HCD spectra. Interestingly, we also observed the diagnostic ion of ADP with the additional phosphate from NS2 deconjugation (Figure 3D, m8-P+), which could serve as a distinct diagnostic ion for MARylated peptides in our workflow. Taken together, the biochemical and mass spectrometry data provided a proof-of-principle that adding DrPARG after ELTA-labeling by OAS1 and deconjugation by NS2 can produce two distinct signals corresponding to the different forms of ADP-ribosylation.

Identifying MARylated and PARylated Forms from ADP-Ribosylated Peptide Standards

Since we were able to enrich a MARylated peptide standard on DBCO-agarose and deconjugate it with NS2 (Figure 2D,E), we next tested whether our triple enzymatic approach could enrich for and generate two distinct mass tags from MARylated and PARylated peptides enriched from a complex mixture. We hypothesized that with our triple enzymatic approach we would identify the MARylated peptide with a unique mass tag of ADPr-P and the PARylated peptide with a unique mass tag of ADPr (Figure 3A). A synthetic MARylated peptide from PARP1 (called JV-522) and a synthetic PARylated peptide from histone H3—a mixture of the peptide with an estimated 30% containing 1 ADPr unit and 70% containing 2−5 ADPr units[33] (called H3(1−20)S10arn)—were spiked into a background of H_2O_2-treated HeLa cell lysate peptides (Figure 4A). For the MARylated standard, we observed the expected mass shift for ADPr-P. The unprocessed JV-522 was minimally carried through the workflow, with a signal less than 3 orders of magnitude lower than the expected ADPr-P signal for the MARylated peptide processed by dELTA-MS (Figure S3). For the PARylated standard, we observed the expected mass shift for ADPr. We did not observe H3(1−20)S10arn with the ADPr-P modification, indicating the estimated 30% of the standard peptide containing 1 ADPr unit was below the limit of detection for our workflow. Sufficient fragments were obtained for the +2 and +3 species of JV-522 and the +6 species of H3(1−20)S10arn in all three technical replicates for each experiment to allow sequence identity confirmations by EThcD fragments as well as modification localization for both ADPr-P and ADPr motifs, respectively (Figure S4). In addition, for the PARylated peptide, additional sequencing ions were observed for the peptide attached to a remainder fragment of ADPr (Figure S5), likely due to the supplemented collision energy, highlighting the complexity of MS2 spectra with this labile modification.

CONCLUSIONS

We present a novel process that allows for reversible labeling of ADP-ribosylation with our ELTA technique, followed by our dELTA method to deconjugate ADP-ribosylation using NS2. Coupled with mass spectrometry, our dELTA-MS approach enables us to preserve information about the native form of ADP-ribosylation associated with the modification site within a single proteomics experiment. As proof of principle, we have shown that NS2 leaves a signature phosphate on the terminal ADP-ribose when cleaving the ELTA label from peptide-conjugated ADP-ribose monomers and polymers. By further incorporating DrPARG treatment into our workflow, this signature phosphate can be used to create two distinct mass tags that differentiate between sites that were originally MARylated and PARylated (Figure 4).

One complexity of ADP-ribosylation is that it can modify nine different amino acids with distinct chemical properties. Recent data suggest that different lengths of ADP-ribose units may be attached to different sites. For example, during DNA damage, serine seems to be predominantly MARylated after 10 min of oxidative stress, while aspartate and glutamate are predominantly PARylated.[42] Therefore, our dELTA-MS workflow could be used to systematically analyze these variations. To achieve this, we need to consider two different factors. First, we must ensure that the enrichment workflow does not introduce a bias against any specific amino acid linkage to ADP-ribosylation. Aspartate and glutamate sites, in particular, are sensitive to basic pH.[43] Therefore, all steps of our enrichment workflow, except for cell lysis, were performed at pH 7.5 to minimize hydrolysis of ADP-ribosylation on acidic residues. Second, different ADP-ribose hydrolases have varying specificities. For example, macrodomains remove ADP-ribose from aspartate and glutamate, while ARH3 targets serine. Previously, data showed that human PARG only cleaves glycosidic bonds between ADP-ribose units and cannot remove the monomer proximal to the amino acid. However, a recent study indicated that human PARG can also remove MARylation from aspartate and glutamate when used at a high concentration (10 μM) or for a prolonged incubation period (>1 h).[42] Here, we utilize PARG from *D. radiodurans*. Despite several conserved contacts of both PARG homologues to ADP-ribose, this bacterial PARG does not remove MARylation from aspartate or glutamate at the concentration and reaction conditions used in our workflow.[30]

Although no proteomics methods have been developed to identify ADP-ribosylation forms, existing chemical methods, such as boronate agarose,[18] and biological reagents, such as the Af1521 macrodomain[41] or antibodies,[15] can enrich and elute them. Our dELTA-MS approach is unique in adding a signature phosphate during release from enrichment, allowing us to differentiate between forms after DrPARG treatment. While our method cannot distinguish individual lengths of ADP-ribose, it presents a compromise of retaining information about the ADP-ribosylation forms at individual sites in a simplified, binary manner.

Ideally, MS techniques should be developed to estimate the length of ADP-ribose units on individual amino acids. Technology used to sequence glycan structure and identify glycopeptides could be adapted to study ADP-ribosylated peptides, such as using information from diagnostic ions or fragment ions,[44,45] separation techniques that can resolve isomers,[45−49] or specialized data acquisition approaches[50−52] and database searching.[53] Similar to glycoproteomics,[54] another complexity in studying ADP-ribosylation is that a peptide's signal could be distributed over multiple PAR lengths, diluting the signal of an already low abundant modification. Additionally, determining the length of ADP-ribosylation faces challenges because, unlike glycan sequencing,[54] it must contend with numerous negative charges, which

https://doi.org/10.1021/acs.jproteome.4c00890
J. Proteome Res. 2025, 24, 1791−1803

can limit ionization of PARylated peptides in the positive ionization mode.

In summary, dELTA-MS offers the first approach to connect ADP-ribosylation sites to their specific forms. We demonstrate the feasibility of this workflow for proteomic analyses using proof-of-principle peptide standards. Applying this method to proteome-wide analyses in lysates could offer deeper insights into trends and patterns of ADP-ribosylation by identifying consensus sequences for MARylation and PARylation, determining the preferred substrates of MARylating or PARylating ADP-ribosyltransferases, and analyzing the ratio of MARylation to PARylation sites. These analyses open up the possibilities to reveal the fundamental biology of ADP-ribosylation and explore its dysregulation, in terms of both sites and forms, associated with the progression of diseases such as cancer, neurodegeneration, and viral infections.

■ LIMITATIONS

While the current workflow demonstrates the feasibility of identifying site-specific ADP-ribosylation and associated form information, it is not yet optimized for high-throughput quantitative analysis or scaled to detect low-abundance ADP-ribosylated peptides. Future efforts will focus on improving workflow efficiency and reproducibility to mitigate sample losses and reduce variability across steps such as labeling, enrichment, and deconjugation. Once optimized, endogenous ADP-ribosylation sites and forms can be identified using a labile search in FragPipe with mass offsets 621.0274 (ADPr-P/MAR site) and 541.0611 (ADPr/PAR site) on DESKTYRCH. However, searching for two offset masses across nine potential amino acids may increase ambiguity due to inflation of the search space, which can have downstream effects on false discovery rates. To address this, Percolator in FragPipe is used to filter all output results for 1% FDR, and modification sites of interest should be confirmed using the manual validation.

■ ASSOCIATED CONTENT

Supporting Information

The Supporting Information is available free of charge at https://pubs.acs.org/doi/10.1021/acs.jproteome.4c00890.

Figure S1: Uncropped gel related to Figure 2. Figure S2: Uncropped gel related to Figure 3. Figure S3: Minimal nonspecific carryover of JV-522 through the dELTA-MS workflow. Figure S4: Representative MS2 spectra of the standard peptides observed in all three technical replicates; related to Figure 4. Figure S5: Remainder ions observed for H3(1−20)S10arn peptide processed by dELTA-MS; related to Figure 4 (PDF)

■ AUTHOR INFORMATION

Corresponding Authors

Benjamin C. Orsburn − *Department of Pharmacology and Chemical Biology, University of Pittsburgh, Pittsburgh, Pennsylvania 15260, United States*; Email: orsburn@pitt.edu

Anthony K. L. Leung − *Department of Biochemistry and Molecular Biology, Bloomberg School of Public Health, Department of Molecular Biology and Genetics, School of Medicine, Department of Genetic Medicine, School of Medicine, and Department of Oncology, School of Medicine, Johns Hopkins University, Baltimore, Maryland 21205, United States*; orcid.org/0000-0001-5569-4036; Email: anthony.leung@jhu.edu

Authors

Isabel R. Uribe − *Department of Biochemistry and Molecular Biology, Bloomberg School of Public Health, Johns Hopkins University, Baltimore, Maryland 21205, United States*

Emily Zahn − *Department of Biochemistry and Molecular Biophysics, Washington University School of Medicine, St. Louis, Missouri 63110, United States*; orcid.org/0009-0009-0431-5820

Richard Searfoss − *Department of Biochemistry and Molecular Biophysics, Washington University School of Medicine, St. Louis, Missouri 63110, United States*

Han-Byeol Kim − *Department of Neurology, Institute for Cell Engineering Johns Hopkins University, Baltimore, Maryland 21205, United States*

Morgan Dasovich − *Department of Biochemistry and Molecular Biology, Bloomberg School of Public Health, Johns Hopkins University, Baltimore, Maryland 21205, United States*

Jim Voorneveld − *Gorlaeus Laboratories, Leiden Institute of Chemistry, Leiden University, 2333 CC Leiden, The Netherlands*

Sabrina R. Hunt − *EpiCypher Inc., Durham, North Carolina 27709, United States*; orcid.org/0000-0003-1873-3846

Ugochi C. Onuoha − *EpiCypher Inc., Durham, North Carolina 27709, United States*; orcid.org/0009-0002-4132-0054

Catherine Valadez − *Department of Biochemistry, University of Texas Southwestern Medical Center, Dallas, Texas 75390, United States*

Dmitri V. Filippov − *Gorlaeus Laboratories, Leiden Institute of Chemistry, Leiden University, 2333 CC Leiden, The Netherlands*

Chan Hyun Na − *Department of Neurology, Institute for Cell Engineering Johns Hopkins University, Baltimore, Maryland 21205, United States*; orcid.org/0000-0002-3622-2938

Benjamin A. Garcia − *Department of Biochemistry and Molecular Biophysics, Washington University School of Medicine, St. Louis, Missouri 63110, United States*; orcid.org/0000-0002-2306-1207

Complete contact information is available at: https://pubs.acs.org/10.1021/acs.jproteome.4c00890

Notes

The authors declare the following competing financial interest(s): EpiCypher is a commercial developer and supplier of the H3(1-20)S10arn peptide used in this study. Sabrina R. Hunt and Ugochi C. Onuoha are employed by (and own shares in) EpiCypher. A patent application on dELTA has been filed.

■ ACKNOWLEDGMENTS

We thank Dr. Namandjé Bumpus, Dr. Stephen Fried, and Dr. Jennifer Kavran for guidance on research progress during the development of this workflow. We thank Dr. Joe Fisher for his suggestion during a lab retreat to add PARG after NS2 treatment. We thank Dr. Andy Hsu for providing the expression construct of DrPARG and Dr. Harry Greenberg for generating the HisSUMO-NS2 plasmid. Work at the Leung lab was funded by F31GM143918 awarded to I.R.U. and

https://doi.org/10.1021/acs.jproteome.4c00890
J. Proteome Res. 2025, 24, 1791−1803

R01GM104135 awarded to A.K.K.L. Work at the Garcia lab was funded by National Institutes of Health grants R01HD106051 and R01AI118891 awarded to B.A.G. Work at the Filippov lab was funded by Leiden Institute of Chemistry. Work at the Liszczak lab was supported by NIH grant R35GM147140. Work at EpiCypher, Inc. was supported by NIH grant R44GM153000. We acknowledge support of the shared instrumentation grant S10OD021844 for experiments done with the Orbitrap Fusion Lumos Mass Spectrometer.

REFERENCES

(1) Lüscher, B.; Bütepage, M.; Eckei, L.; Krieg, S.; Verheugd, P.; Shilton, B. H. ADP-Ribosylation, a Multifaceted Posttranslational Modification Involved in the Control of Cell Physiology in Health and Disease. *Chem. Rev.* **2018**, *118*, 1092.
(2) Palazzo, L.; Mikolčević, P.; Mikoč, A.; Ahel, I. ADP-ribosylation signalling and human disease. *Open Biol.* **2019**, *9*, 190041.
(3) Cohen, M. S.; Chang, P. Insights into the biogenesis, function, and regulation of ADP-ribosylation. *Nat. Chem. Biol.* **2018**, *14*, 236.
(4) Gupte, R.; Liu, Z.; Kraus, W. L. PARPs and ADP-ribosylation: recent advances linking molecular functions to biological outcomes. *Genes Dev.* **2017**, *31*, 101−126.
(5) Leung, A. K. L. Poly(ADP-ribose): A Dynamic Trigger for Biomolecular Condensate Formation. *Trends Cell Biol.* **2020**, *30*, 370.
(6) Lüscher, B.; Ahel, I.; Altmeyer, M.; Ashworth, A.; Bai, P.; Chang, P.; Cohen, M.; Corda, D.; Dantzer, F.; Daugherty, M. D.; Dawson, T. M.; Dawson, V. L.; Deindl, S.; Fehr, A. R.; Feijs, K. L. H.; Filippov, D. V.; Gagné, J.; Grimaldi, G.; Guettler, S.; Hoch, N. C.; Hottiger, M. O.; Korn, P.; Kraus, W. L.; Ladurner, A.; Lehtiö, L.; Leung, A. K. L.; Lord, C. J.; Mangerich, A.; Matic, I.; Matthews, J.; Moldovan, G.; Moss, J.; Natoli, G.; Nielsen, M. L.; Niepel, M.; Nolte, F.; Pascal, J.; Paschal, B. M.; Pawłowski, K.; Poirier, G. G.; Smith, S.; Timinszky, G.; Wang, Z.; Yélamos, J.; Yu, X.; Zaja, R.; Ziegler, M. ADP-ribosyltransferases, an update on function and nomenclature. *FEBS J.* **2022**, *289*, 7399.
(7) Aberle, L.; Krüger, A.; Reber, J. M.; Lippmann, M.; Hufnagel, M.; Schmalz, M.; Trussina, I. R. E. A.; Schlesiger, S.; Zubel, T.; Schütz, K.; Marx, A.; Hartwig, A.; Ferrando-May, E.; Bürkle, A.; Mangerich, A. PARP1 catalytic variants reveal branching and chain length-specific functions of poly(ADP-ribose) in cellular physiology and stress response. *Nucleic Acids Res.* **2020**, *48*, 10015.
(8) Bonfiglio, J. J.; Fontana, P.; Zhang, Q.; Colby, T.; Gibbs-Seymour, I.; Atanassov, I.; Bartlett, E.; Zaja, R.; Ahel, I.; Matic, I. Serine ADP-Ribosylation Depends on HPF1. *Mol. Cell* **2017**, *65*, 932.
(9) Leidecker, O.; Bonfiglio, J. J.; Colby, T.; Zhang, Q.; Atanassov, I.; Zaja, R.; Palazzo, L.; Stockum, A.; Ahel, I.; Matic, I. Serine is a new target residue for endogenous ADP-ribosylation on histones. *Nat. Chem. Biol.* **2016**, *12*, 998.
(10) Gibbs-Seymour, I.; Fontana, P.; Rack, J. G. M.; Ahel, I. HPF1/C4orf27 Is a PARP-1-Interacting Protein that Regulates PARP-1 ADP-Ribosylation Activity. *Mol. Cell* **2016**, *62*, 432.
(11) Ando, Y.; Elkayam, E.; Mcpherson, R. L.; Dasovich, M.; Cheng, S.; Voorneveld, J.; Filippov, D. V.; Ong, S.; Joshua-Tor, L.; Leung, A. K. L. ELTA: Enzymatic Labeling of Terminal ADP-Ribose. *Mol. Cell* **2019**, *73*, 845.
(12) Fahrer, J.; Kranaster, R.; Altmeyer, M.; Marx, A.; Bürkle, A. Quantitative analysis of the binding affinity of poly(ADP-ribose) to specific binding proteins as a function of chain length. *Nucleic Acids Res.* **2007**, *35*, No. e143.
(13) Fahrer, J.; Popp, O.; Malanga, M.; Beneke, S.; Markovitz, D. M.; Ferrando-May, E.; Bürkle, A.; Kappes, F. High-Affinity Interaction of Poly(ADP-ribose) and the Human DEK Oncoprotein Depends upon Chain Length. *Biochemistry* **2010**, *49*, 7119.
(14) Reber, J. M.; Mangerich, A. Why structure and chain length matter: on the biological significance underlying the structural heterogeneity of poly(ADP-ribose). *Nucleic Acids Res.* **2021**, *49*, 8432.
(15) Bonfiglio, J. J.; Leidecker, O.; Dauben, H.; Longarini, E. J.; Colby, T.; San Segundo-Acosta, P.; Perez, K. A.; Matic, I. An HPF1/PARP1-Based Chemical Biology Strategy for Exploring ADP-Ribosylation. *Cell* **2020**, *183*, 1086.
(16) Dani, N.; Stilla, A.; Marchegiani, A.; Tamburro, A.; Till, S.; Ladurner, A. G.; Corda, D.; Di Girolamo, M. Combining affinity purification by ADP-ribose-binding macro domains with mass spectrometry to define the mammalian ADP-ribosyl proteome. *Proc. Natl. Acad. Sci. U.S.A.* **2009**, *106*, 4243−4248.
(17) Jungmichel, S.; Rosenthal, F.; Altmeyer, M.; Lukas, J.; Hottiger, M. O.; Nielsen, M. L. Proteome-wide Identification of Poly(ADP-Ribosyl)ation Targets in Different Genotoxic Stress Responses. *Mol. Cell* **2013**, *52*, 272.
(18) Zhang, Y.; Wang, J.; Ding, M.; Yu, Y. Site-specific characterization of the Asp- and Glu-ADP-ribosylated proteome. *Nat. Methods* **2013**, *10*, 981.
(19) Carter-O'Connell, I.; Jin, H.; Morgan, R. K.; David, L. L.; Cohen, M. S. Engineering the Substrate Specificity of ADP-Ribosyltransferases for Identifying Direct Protein Targets. *J. Am. Chem. Soc.* **2014**, *136*, 5201.
(20) Rodriguez, K. M.; Buch-Larsen, S. C.; Kirby, I. T.; Siordia, I. R.; Hutin, D.; Rasmussen, M.; Grant, D. M.; David, L. L.; Matthews, J.; Nielsen, M. L.; Cohen, M. S. Chemical genetics and proteome-wide site mapping reveal cysteine MARylation by PARP-7 on immune-relevant protein targets. *eLife* **2021**, *10*, 1.
(21) Daniels, C. M.; Ong, S.; Leung, A. K. L. Phosphoproteomic Approach to Characterize Protein Mono- and Poly(ADP-ribosyl)-ation Sites from Cells. *J. Proteome Res.* **2014**, *13*, 3510.
(22) Vivelo, C. A.; Leung, A. K. L. Proteomics approaches to identify mono-(ADP-ribosyl)ated and poly(ADP-ribosyl)ated proteins. *Proteomics* **2015**, *15*, 203.
(23) Dasovich, M.; Leung, A. K. L. PARPs and ADP-ribosylation: Deciphering the complexity with molecular tools. *Mol. Cell* **2023**, *83*, 1552.
(24) Larsen, S. C.; Hendriks, I. A.; Lyon, D.; Jensen, L. J.; Nielsen, M. L. Systems-wide Analysis of Serine ADP-Ribosylation Reveals Widespread Occurrence and Site-Specific Overlap with Phosphorylation. *Cell Rep.* **2018**, *24*, 2493.
(25) McPherson, R. L.; Ong, S.; Leung, A. K. L. Ion-Pairing with Triethylammonium Acetate Improves Solid-Phase Extraction of ADP-Ribosylated Peptides. *J. Proteome Res.* **2020**, *19*, 984.
(26) Daniels, C. M.; Thirawatananond, P.; Ong, S.; Gabelli, S. B.; Leung, A. K. L. Nudix hydrolases degrade protein-conjugated ADP-ribose. *Sci. Rep.* **2015**, *5*, 18271.
(27) Drappier, M.; Michiels, T. Inhibition of the OAS/RNase L pathway by viruses. *Curr. Opin. Virol.* **2015**, *15*, 19.
(28) Zhao, L.; Jha, B. K.; Wu, A.; Elliott, R.; Ziebuhr, J.; Gorbalenya, A. E.; Silverman, R. H.; Weiss, S. R. Antagonism of the Interferon-Induced OAS-RNase L Pathway by Murine Coronavirus ns2 Protein Is Required for Virus Replication and Liver Pathology. *Cell Host Microbe* **2012**, *11*, 607.
(29) Snijder, E. J.; Bredenbeek, P. J.; Dobbe, J. C.; Thiel, V.; Ziebuhr, J.; Poon, L. L. M.; Guan, Y.; Rozanov, M.; Spaan, W. J. M.; Gorbalenya, A. E. Unique and Conserved Features of Genome and Proteome of SARS-coronavirus, an Early Split-off From the Coronavirus Group 2 Lineage. *J. Mol. Biol.* **2003**, *331*, 991.
(30) Cho, C.; Chien, C.; Chiu, Y.; Lin, M.; Hsu, C. Structural and biochemical evidence supporting poly ADP-ribosylation in the bacterium Deinococcus radiodurans. *Nat. Commun.* **2019**, *10*, 1491.
(31) Voorneveld, J.; Rack, J. G. M.; Ahel, I.; Overkleeft, H. S.; Van Der Marel, G. A.; Filippov, D. V. Synthetic α- and β-Ser-ADP-ribosylated Peptides Reveal α-Ser-ADPr as the Native Epimer. *Org. Lett.* **2018**, *20*, 4140.
(32) Voorneveld, J.; Rack, J. G. M.; Van Gijlswijk, L.; Meeuwenoord, N. J.; Liu, Q. S.; Overkleeft, H. S.; Van Der Marel, G. A.; Ahel, I.; Filippov, D. V. Molecular Tools for the Study of ADP-Ribosylation: A Unified and Versatile Method to Synthesise Native Mono-ADP-Ribosylated Peptides. *Chem.—Eur. J.* **2021**, *27*, 10621−10627.
(33) Mohapatra, J.; Tashiro, K.; Beckner, R. L.; Sierra, J.; Kilgore, J. A.; Williams, N. S.; Liszczak, G. Serine ADP-ribosylation marks

https://doi.org/10.1021/acs.jproteome.4c00890
J. Proteome Res. 2025, 24, 1791−1803

nucleosomes for ALC1-dependent chromatin remodeling. *eLife* **2021**, *10*, 1.
(34) Collins, A.; Jones, A. R. phpMs: A PHP-Based Mass Spectrometry Utilities Library. *J. Proteome Res.* **2018**, *17*, 1309.
(35) Brademan, D. R.; Riley, N. M.; Kwiecien, N. W.; Coon, J. J. Interactive Peptide Spectral Annotator: A Versatile Web-based Tool for Proteomic Applications. *Mol. Cell. Proteomics* **2019**, *18*, S193.
(36) Dickman, M. J.; Hornby, D. P. Enrichment and analysis of RNA centered on ion pair reverse phase methodology. *RNA* **2006**, *12*, 691.
(37) Aboelnga, M. M.; Wetmore, S. D. Unveiling a Single-Metal-Mediated Phosphodiester Bond Cleavage Mechanism for Nucleic Acids: A Multiscale Computational Investigation of a Human DNA Repair Enzyme. *J. Am. Chem. Soc.* **2019**, *141*, 8646.
(38) Roth-Cross, J. K.; Stokes, H.; Chang, G.; Chua, M. M.; Thiel, V.; Weiss, S. R.; Gorbalenya, A. E.; Siddell, S. G. Organ-Specific Attenuation of Murine Hepatitis Virus Strain A59 by Replacement of Catalytic Residues in the Putative Viral Cyclic Phosphodiesterase ns2. *J. Virol.* **2009**, *83*, 3743.
(39) Asthana, A.; Gaughan, C.; Dong, B.; Weiss, S. R.; Silverman, R. H. Specificity and Mechanism of Coronavirus, Rotavirus, and Mammalian Two-Histidine Phosphodiesterases That Antagonize Antiviral Innate Immunity. *mBio* **2021**, *12*, No. e0178121.
(40) Szaéjli, E.; Feheér, T.; Medzihradszky, K. F. Investigating the Quantitative Nature of MALDI-TOF MS. *Mol. Cell. Proteomics* **2008**, *7*, 2410.
(41) Hendriks, I. A.; Larsen, S. C.; Nielsen, M. L. An Advanced Strategy for Comprehensive Profiling of ADP-ribosylation Sites Using Mass Spectrometry-based Proteomics. *Mol. Cell. Proteomics* **2019**, *18*, 1010−1026.
(42) Longarini, E. J.; Matić, I. Preserving ester-linked modifications reveals glutamate and aspartate mono-ADP-ribosylation by PARP1 and its reversal by PARG. *Nat. Commun.* **2024**, *15*, 4239.
(43) Tashiro, K.; Wijngaarden, S.; Mohapatra, J.; Rack, J. G. M.; Ahel, I.; Filippov, D. V.; Liszczak, G. Chemoenzymatic and Synthetic Approaches To Investigate Aspartate- and Glutamate-ADP-Ribosylation. *J. Am. Chem. Soc.* **2023**, *145*, 14000.
(44) Ashwood, C.; Lin, C.; Thaysen-Andersen, M.; Packer, N. H. Discrimination of Isomers of Released N- and O-Glycans Using Diagnostic Product Ions in Negative Ion PGC-LC-ESI-MS/MS. *J. Am. Soc. Mass Spectrom.* **2018**, *29*, 1194.
(45) Helms, A.; Brodbelt, J. S. Mass Spectrometry Strategies for O-Glycoproteinics. *Cells* **2024**, *13*, 394.
(46) Stavenhagen, K.; Hinneburg, H.; Kolarich, D.; Wuhrer, M. Site-Specific N- and O-Glycopeptide Analysis Using an Integrated C18-PGC-LC-ESI-QTOF-MS/MS Approach. In *High-Throughput Glycomics and Glycoproteinics: Methods and Protocols*; Lauc, G., Wuhrer, M., Eds.; Springer: New York, 2017; p 109.
(47) Kammeijer, G. S. M.; Jansen, B. C.; Kohler, I.; Heemskerk, A. A. M.; Mayboroda, O. A.; Hensbergen, P. J.; Schappler, J.; Wuhrer, M. Sialic acid linkage differentiation of glycopeptides using capillary electrophoresis − electrospray ionization − mass spectrometry. *Sci. Rep.* **2017**, *7*, 3733.
(48) Mukherjee, S.; Jankevics, A.; Busch, F.; Lubeck, M.; Zou, Y.; Kruppa, G.; Heck, A. J. R.; Scheltema, R. A.; Reiding, K. R. Oxonium Ion−Guided Optimization of Ion Mobility−Assisted Glycoproteinics on the timsTOF Pro. *Mol. Cell. Proteomics* **2023**, *22*, 100486.
(49) Bechtella, L.; Chunsheng, J.; Fentker, K.; Ertürk, G. R.; Safferthal, M.; Polewski, Ł.; Götze, M.; Graeber, S. Y.; Vos, G. M.; Struwe, W. B.; Mall, M. A.; Mertins, P.; Karlsson, N. G.; Pagel, K. Ion mobility-tandem mass spectrometry of mucin-type O-glycans. *Nat. Commun.* **2024**, *15*, 2611.
(50) Armony, G.; Brehmer, S.; Srikumar, T.; Pfennig, L.; Zijlstra, F.; Trede, D.; Kruppa, G.; Lefeber, D. J.; Van Gool, A. J.; Wessels, H. J. C. T. The GlycoPaSER Prototype as a Real-Time N-Glycopeptide Identification Tool Based on the PaSER Parallel Computing Platform. *Int. J. Mol. Sci.* **2023**, *24*, 7869.
(51) Woo, C. M.; Iavarone, A. T.; Spiciarich, D. R.; Palaniappan, K. K.; Bertozzi, C. R. Isotope-targeted glycoproteinics (IsoTaG): a mass-independent platform for intact N- and O-glycopeptide discovery and analysis. *Nat. Methods* **2015**, *12*, 561.
(52) Ye, Z.; Vakhrushev, S. Y. The Role of Data-Independent Acquisition for Glycoproteinics. *Mol. Cell. Proteomics* **2021**, *20*, 100042.
(53) Polasky, D. A.; Lu, L.; Yu, F.; Li, K.; Shortreed, M. R.; Smith, L. M.; Nesvizhskii, A. I. Quantitative proteome-wide O-glycoproteomics analysis with FragPipe. *Anal. Bioanal. Chem.* **2025**, *1*, 921−930.
(54) Bagdonaite, I.; Malaker, S. A.; Polasky, D. A.; Riley, N. M.; Schjoldager, K.; Vakhrushev, S. Y.; Halim, A.; Aoki-Kinoshita, K. F.; Nesvizhskii, A. I.; Bertozzi, C. R.; Wandall, H. H.; Parker, B. L.; Thaysen-Andersen, M.; Scott, N. E. Glycoproteinics. *Nat. Rev. Methods Primers* **2022**, *2*, 48.

https://doi.org/10.1021/acs.jproteome.4c00890
J. Proteome Res. 2025, 24, 1791−1803